FUNDAMENTAL STUDIES OF JUMPING-DROP THERMAL DIODES

Chuan-Hua Chen

**Duke University
Office of Research Support
2200 W. Main St, Suite 710
Durham, NC 27708-4677**

29 Feb 2016

Final Report

APPROVED FOR PUBLIC RELEASE; DISTRIBUTION IS UNLIMITED.

**AIR FORCE RESEARCH LABORATORY
Space Vehicles Directorate
3550 Aberdeen Ave SE
AIR FORCE MATERIEL COMMAND
KIRTLAND AIR FORCE BASE, NM 87117-5776**

DTIC COPY

NOTICE AND SIGNATURE PAGE

AFRL-RV-PS-TR-2016-0002 HAS BEEN REVIEWED AND IS APPROVED FOR PUBLICATION IN ACCORDANCE WITH ASSIGNED DISTRIBUTION STATEMENT.

 //SIGNED//   //SIGNED//

ANDREW WILLIAMS   PAUL HAUSGEN, Ph.D.
Program Manager   Technical Advisor, Spacecraft Component Technology

 //SIGNED//

JOHN BEAUCHEMIN
Chief Engineer, Spacecraft Technology Division
Space Vehicles Directorate

REPORT DOCUMENTATION PAGE

Form Approved
OMB No. 0704-0188

1. REPORT DATE *(DD-MM-YYYY)* 29-02-2016	2. REPORT TYPE Final Report	3. DATES COVERED *(From - To)* 20 Feb 2015-20 Feb 2016
4. TITLE AND SUBTITLE Fundamental Studies of Jumping-Drop Thermal Diodes		**5a. CONTRACT NUMBER** FA9453-15-1-0312
		5b. GRANT NUMBER
		5c. PROGRAM ELEMENT NUMBER 61102F
6. AUTHOR(S) Chuan-Hua Chen		**5d. PROJECT NUMBER** MIPR
		5e. TASK NUMBER PPM00014700
		5f. WORK UNIT NUMBER EF126349
7. PERFORMING ORGANIZATION NAME(S) AND ADDRESS(ES) Duke University Office of Research Support 2200 W. Main St, Suite 710 Durham, NC 27708-4677		**8. PERFORMING ORGANIZATION REPORT NUMBER**
9. SPONSORING / MONITORING AGENCY NAME(S) AND ADDRESS(ES) Space Vehicles Directorate Air Force Research Laboratory 3550 Aberdeen Ave SE Kirtland AFB, NM 87117-5776		**10. SPONSOR/MONITOR'S ACRONYM(S)** AFRL/RVSV
		11. SPONSOR/MONITOR'S REPORT NUMBER(S) AFRL-RV-PS-TR-2016-0002

12. DISTRIBUTION / AVAILABILITY STATEMENT

Approved for public release; distribution is unlimited.

13. SUPPLEMENTARY NOTES

14. ABSTRACT

In this exploratory project, the performance of the planar jumping-drop thermal diode was studied after freeze-thaw cycles. The thermal diode consisted of two parallel plates, one superhydrophobic and one superhydrophilic, separated by a thermally insulating gasket which also provided a vacuum seal. In the forward mode when the superhydrophobic plate was colder, the self-propelled jumping of condensate drops on the superhydrophobic surface returned the working fluid to the opposing superhydrophilic surface. Both the galvanic superhydrophobic surface and sintered superhydrophilic surface were verified to survive a freeze-thaw cycle. However, the flat gasket for vacuum seal introduced leakage of noncondensable gases after a freeze-thaw cycle. With a modified gasket design, the jumping-drop thermal diode should be suitable for freeze-thaw conditions.

15. SUBJECT TERMS
Jumping-Drop Thermal Diode, Heat Switch, Superhydrophobic, Superhydrophilic

16. SECURITY CLASSIFICATION OF:			17. LIMITATION OF ABSTRACT	18. NUMBER OF PAGES	19a. NAME OF RESPONSIBLE PERSON Andrew Williams
a. REPORT Unclassified	**b. ABSTRACT** Unclassified	**c. THIS PAGE** Unclassified	Unlimited	24	**19b. TELEPHONE NUMBER** *(include area code)*

Standard Form 298 (Rev. 8-98)
Prescribed by ANSI Std. Z39.18

(This page intentionally left blank)

TABLE OF CONTENTS

LIST OF FIGURES

Figure **Page**

ACKNOWLEDGMENTS

DISCLAIMER

(This page intentionally left blank)

1 SUMMARY

In this exploratory project, we studied the performance of the jumping-drop thermal diode under freeze-thaw conditions and also evaluated its packaging for potential independent testing. The thermal diode consists of two parallel plates separated by a thermally insulating gasket, which also provides a vacuum seal. In the forward mode, the self-propelled jumping of condensate drops on the superhydrophobic plate is used to return the working fluid to the hotter superhydrophilic plate, resulting in effective phase-change heat transfer. In the reverse mode, the jumping return mechanism ceases to function when the working fluid condenses on the colder superhydrophilic plate, leading to ineffective heat transport by vapor conduction. **Our major findings and recommendations** are summarized below:

- *The galvanic superhydrophobic and sintered superhydrophilic surfaces survived a freeze-thaw cycle.* Although a major concern at the beginning of this study, the durability of the superhydrophobic surface was confirmed by our tests. In the future, repeated freeze-thaw cycles should be introduced to study long-term durability for space applications.

- *The flat gasket for vacuum seal introduced leakage of noncondensable gases after a freeze-thaw cycle.* Although the flat gasket design worked fine at room temperature and above, it was not suitable under freezing conditions. The inadequacy of the flat gasket was verified on many alternative materials such as ethylene-propylene-diene monomer (EPDM), Buna-N and Neopreene. In the future, O-rings should be evaluated instead of flat gaskets, perhaps with a material exhibiting good vacuum performance as identified in this study.

- *The present thermal diode design after a crimp-seal survived the shipping test*, including repeated dropping to ground in a postal package.

Since the surface coating passed the freeze-thaw tests but the flat gasket turned out to be problematic, the program tasks have been modified in consultation with the program managers at AFRL. **Our progress** is assessed below against the original program tasks:

Q1. Construct the jumping-drop thermal diode and assemble the characterization setup. Study the effect of freeze-thaw cycles on the wettability and stability of both superhydrophobic and superhydrophilic plates, and adapt coating recipes as needed.

Accomplished. The durability of the superhydrophobic and superhydrophilic surfaces was verified under freeze-thaw conditions, but the flat gasket for vacuum seal was shown to exhibit poor vacuum performance after a freeze-thaw cycle.

Q2. Integrate transparent sidewalls into jumping-drop vapor chambers and assemble high-speed optical imaging for transient studies involving freeze-thaw cycles. Study frozen startup behavior with and against gravity, both thermally and optically.

Accomplished. The diode was tested both thermally and optically, but priority was given to identification and testing of alternative gasket materials. (The tests were mainly against gravity, which is the most demanding orientation for jumping return.)

Q3. Evaluate the performance of thermal diodes with respect to repeated freeze-thaw cycles at different orientations, and adjust the working fluid as needed. Summarize research findings in light of potential space applications.

Accomplished. The diode was tested after shipment or freeze-thaw. The diode survived conditions simulating postal shipment, but the performance degraded after a freeze-thaw cycle. The degradation was attributed to air leakage by the flat gasket.

2 INTRODUCTION

The overall objective of this work is to study the performance of jumping-drop thermal diodes after freeze-thaw cycles, which is important in the context of space platforms that require reliable performance following frozen startups. Schematically shown in Figure 1, the jumping-drop thermal diode under investigation consists of a planar vapor chamber with opposing superhydrophobic and superhydrophilic plates [1]. The plates are separated by a thermally insulating gasket which also provides a vacuum seal. When the superhydrophilic surface is heated with respect to the superhydrophobic one (forward mode, Figure 1a), the evaporating water carries heat away from the superhydrophilic surface and the vapor condenses on the superhydrophobic surface; the self-propelled jumping motion returns the condensed drops back to the evaporator [2], completing the circulation of working fluid with highly effective phase-change heat transfer. When the superhydrophilic surface is cooler (reverse mode, Figure 1b), liquid water is trapped by it and no phase-change heat transfer takes place; heat mainly escapes through ineffective conduction across the vacuum gasket and vapor space. Note that the wick structure in our thermal diode serves to evenly distribute the working liquid *within* the superhydrophilic surface and hold it against gravity. In contrast, the wick in conventional heat pipes is playing the additional role of returning condensate to the evaporator by capillary action. Note that the sidewalls are important for thermal isolation and vacuum sealing, and can be made transparent for optical access inside the chamber.
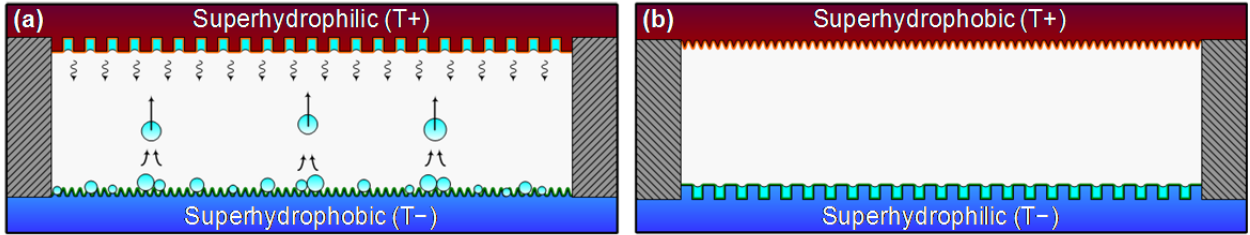
Figure 1. Schematic of the planar jumping-drop thermal diode (not to scale): (a) Forward mode with self-propelled jumping drops returning the working fluid from the colder superhydrophobic surface; (b) Reverse mode with liquid trapped by the colder superhydrophilic surface.

Our phase-change thermal diode is inherently planar with an orientation-independent diodicity (rectification coefficient) of over 100. The diodicity η is defined as

$$\eta = \frac{k_f - k_r}{k_r},\tag{1}$$

where k_f and k_r are the effective thermal conductivities in the forward and reverse operating modes, respectively.

3 METHODS, ASSUMPTIONS, AND PROCEDURES

3.1 Fabrication and Assembly

The superhydrophobic surface (Figure 2a) was fabricated using electroless galvanic deposition of silver nanoparticles onto a copper substrate [3], which was subsequently coated with a monolayer of 1-hexadecanethiol. The superhydrophobic plate had two ports for liquid injection and vacuum pumping (visible in Figure 2a inset). The opposing superhydrophilic surface (Figure 2b) consisted of copper wick sintered to a copper plate (commercially available from e.g. Thermacore) and treated with an oxygen plasma or thermal oxidization. The copper plates had a cross-sectional area of $A = 76$ mm $\times$ 76 mm, a thickness of 8.9 mm (superhydrophobic) and 6.4 mm (superhydrophilic), and a thermal conductivity of 390 W/m·K. The plate dimensions were somewhat arbitrary and chosen primarily to facilitate fabrication. The copper wick had an area of $A_w = 61$ mm $\times$ 61 mm, a thickness of $H_w = 1.0$ mm, and a conductivity of approximately $k_w = 38$ W/m·K.

The two parallel plates were then vacuum sealed with a gasket via mechanical compression (Figure 2c). A syringe was used to charge deionized water as the working fluid into the assembled chamber (Figure 3a). A vacuum pump was then used to evacuate the noncondensable gases, including those dissolved in the working fluid. Multiple vacuums could be pulled to ensure complete evacuation of the noncondensables. After charging and testing, the two ports could be crimp-sealed to provide a stand-alone thermal diode.
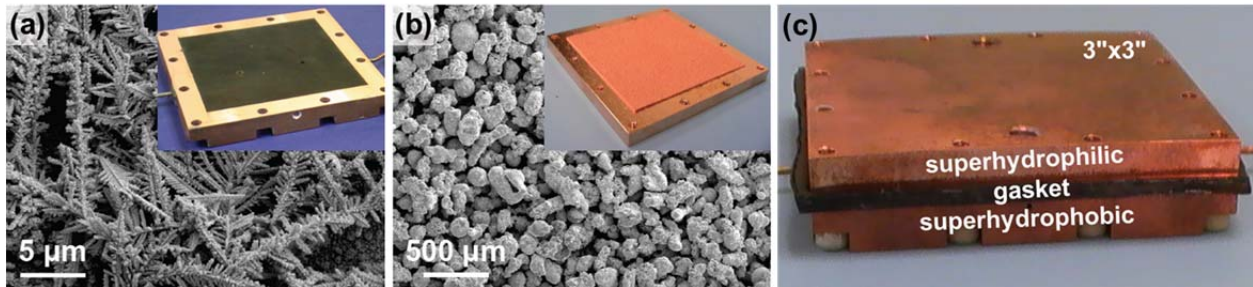
Figure 2. Fabrication of the jumping-drop thermal diode: (a) The superhydrophobic surface with galvanically deposited micro/nano structures; (b) The superhydrophilic surface with sintered copper wick. (c) The two copper plates were mechanically compressed together with a flat gasket for vacuum sealing.

3.2 Characterization Setup

During testing, the parallel-plate diode was subjected to resistive heating on one side, and cold-plate cooling on the other side (Figure 3a). Note that the two copper tubes shown in Figure 3 were used for charging of the working fluid and evacuation of the noncondensable gases. The heating with a specified power Q was provided by three cartridge heaters inserted into a copper plate of the same cross sectional area as the diode (76 mm x 76 mm). The backside of the heater was wrapped with insulating rubber foam to minimize heat leakage. The cooling was provided by a cold plate connected to a refrigerated circulator, with the circulating fluid maintained at a specified temperature T_0. If freeze-thaw testing was needed, the cold plate was first cooled to below 0°C (Figure 3b), and then brought up to a desired temperature of operation.

The thermal diode was tested in both the forward and the reverse modes. In the forward mode (Figure 4a-b), the superhydrophobic surface was at the bottom and cooled, so the jumping drops were moving against gravity. As such, the diode was tested in the most difficult orientation for the jumping return. In the reverse mode (Figure 4c-d), the superhydrophobic surface was at the top and heated, so there would be no jumping drops. Note that the heater plate and the insulating foam were removed from the images in Figure 4 (a) and Figure 4 (c) for clarity.

Figure 3. (a) Test assembly of the thermal diode; (b) Freezing test, where the diode was cooled below freezing temperature *via* the cold plate.

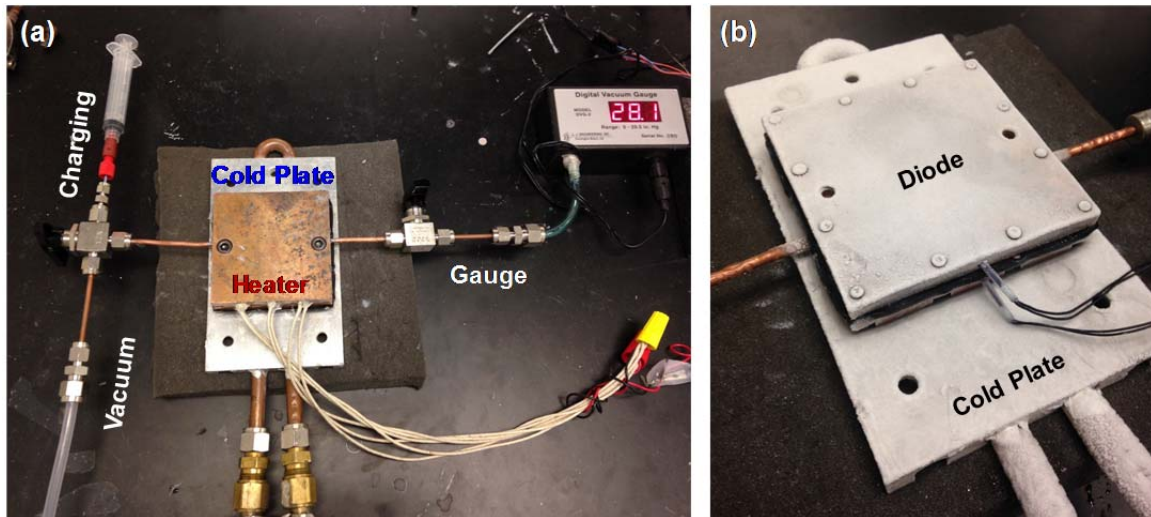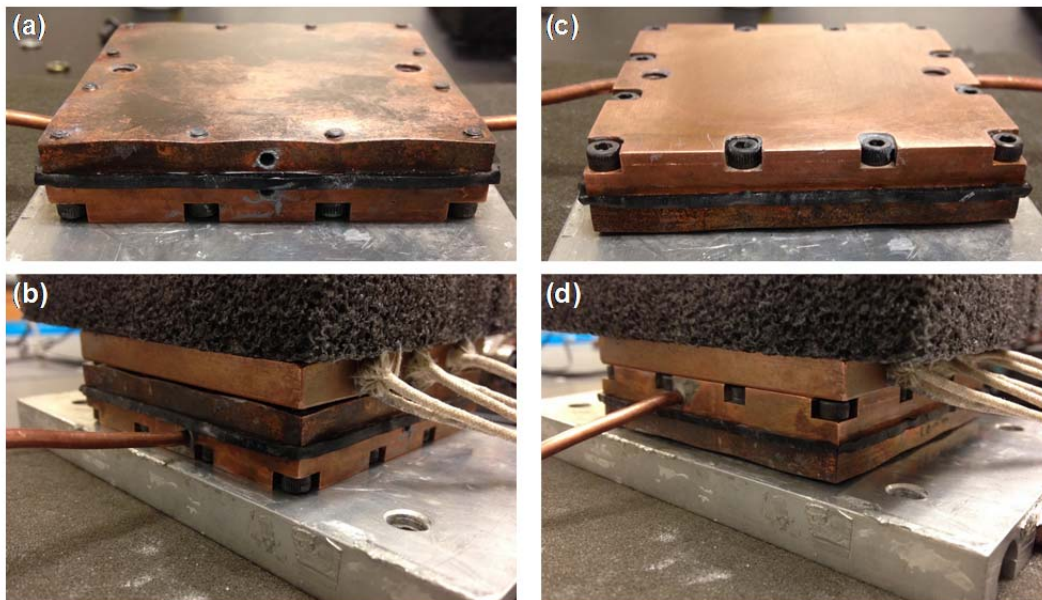**Figure 4.** (a-b) Forward-mode test with the superhydrophobic plate cooled at the bottom; (c-d) Reverse-mode test with the superhydrophobic plate heated at the top.

In Figure 3, the effective conductivity across the vapor chamber was measured by

$$k_{eff} = \frac{HQ}{A\Delta T},$$

(2)

where H was the total height of the wick and the vapor spacing, ΔT was the steady-state temperature drop between the copper plates at a given power input Q, and A was the total cross-sectional area of the plates including the surrounding gasket. Alternatively, an overall heat transfer coefficient was defined as

$$h_o = \frac{Q}{A_w \Delta T},$$

(3)

where the wick area A_w was used. More details of the fabrication, assembly and characterization processes can be found in our prior publication [4], including the degassing procedure to remove noncondensable gases critical for the optimal functioning of the phase-change system and the uncertainty analysis for our experimental system.

4   RESULTS AND DISCUSSION

4.1   Thermal Diode Packaging

In preparation for the independent thermal testing at AFRL, we evaluated the crimp tool (CHA Industries KEL-375) to seal the copper pipes used for charging and evacuation (Figure 5a). When subjected to vacuum tests, the crimped tube showed excellent capability to sustain vacuum.

For the shipping test, the copper pipes were sealed with the crimp tool after their usage in charging and evacuation. The sealed diode was affixed to an aluminum box (Figure 5) and wrapped with packing foam in a cardboard box. The thermal diode package was then tested under conditions simulating postal shipment, e.g. transported in an automobile after being repeatedly dropped to the ground from waist height.
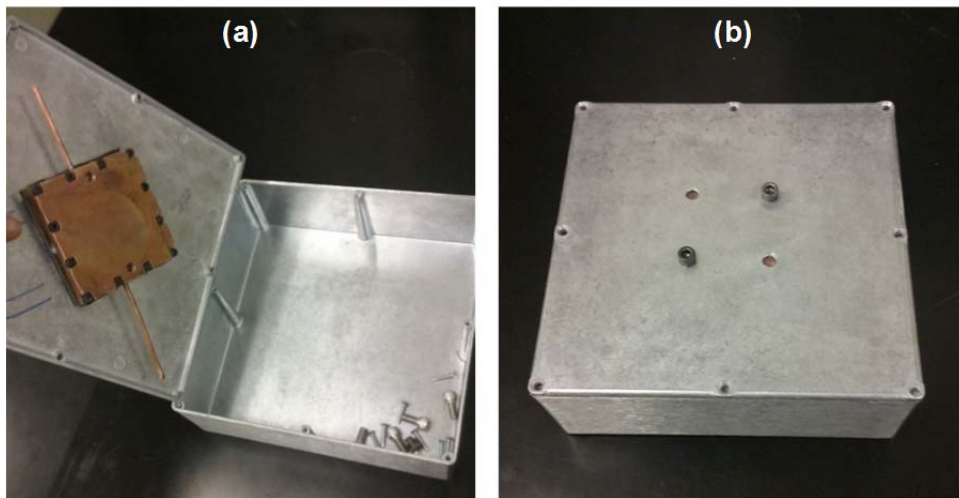

Figure 5. The assembled diode was affixed to an aluminum box and subjected to a shipping test.

4.2 Transparent Vapor Chamber

We previously assembled a vapor chamber with transparent side walls for optical access (Figure 6a). The sidewalls were made of acrylic and the vacuum seal was accomplished through two latex sheets sandwiching the acrylic. With a long exposure time, the jumping drops were captured with streaks indicating the perpendicular jumping return from the superhydrophobic condenser to the superhydrophilic evaporator (against gravity in this case).

To accommodate our new chamber geometry, we made a transparent sidewall by machining a solid acrylic block (Figure 6b). Unfortunately, the mechanical polishing was insufficient to create a smooth sidewall for clear optical access. We shall note that the transparent sidewall was proposed to study potential complications due to frozen startup. Since our work below suggested that the main complication arose from the gasket material, the transparent chamber was no longer a priority.
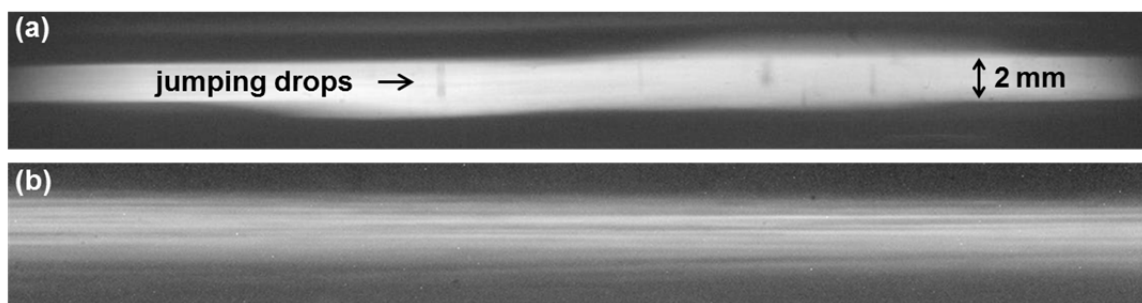
Figure 6. Transparent sidewalls of the vapor chamber for optical access: (a) Smooth sidewall created from an off-the-shelf acrylic tube (b) Rough sidewall created by machining a solid block of acrylic.

4.3 Gasket Materials

4.3.1 Candidate Gasket Materials

In this project, we found that EPDM gasket material could not adequately hold vacuum after a freeze-thaw cycle. As potential alternatives, the following gasket materials of different hardness (in Shore durometer) were tested, at a thickness of 3/32″ unless otherwise noted:

a) EPDM 60A (McMaster Carr 8610K83)

b) Silicone 50A (McMaster Carr 3788T25, 2.5 mm thickness)

c) Silicone 60A (McMaster Carr 8632K43 – 60A)

d) Silicone 70A (McMaster Carr 8632K43 – 70A)

e) Silicone 90A (McMaster Carr 5773T23)

f) Silicone 70A, fiberglass reinforced (McMaster Carr 8612K53)

g) Neoprene 70A (McMaster Carr 9455K12 – 70A)

h) Neoprene 80A (McMaster Carr 9455K12 – 80A)

i) Butyl 60A (McMaster Carr 8609K2, 1/8″ thickness)

j) Viton 75A (McMaster Carr 86075K23)

k) Buna-N 60A (McMaster Carr 8969K56 – 60A)

l) Buna-N 70A (McMaster Carr 8969K56 – 70A)

Among these materials, EPDM 60A was used in our prior research on thermal diode [4]. Silicone was chosen because of its usage as vacuum seals in prior reports of vapor chambers [5]. Neoprene (Polychloroprene) was chosen because of its usage as gasket material in freeze-drying systems [6]. The rest of the materials, including Butyl, Viton (Fluorocarbon), and Buna-N (Nitrile), were chosen according to recommendations of National Aeronautics and Space Administration (NASA)'s "Vacuum seals design criteria" [7]. Note that the NASA document on vacuum seals is mainly concerned with O-rings, and the recommended materials may not be directly applicable since our chamber uses flattened gasket materials.

When the alternative gasket materials were tested, Silicone 50A, 60A and 70A as well as Butyl 60A gaskets were all too soft and were significantly deformed after assembly. For example, a 60A silicone gasket was substantially deformed after the chamber assembly (Figure 7), although its hardness was the same as the EPDM gasket used in Figure 2c and both gaskets were of the same thickness of 3/32″. The fiber-reinforcement of silicone 70A caused air leakage. Viton 75A was mechanically rigid but substantial vacuum loss was observed after a freeze-thaw cycle. The rest of the gasket materials were tested below for their vacuum performance.
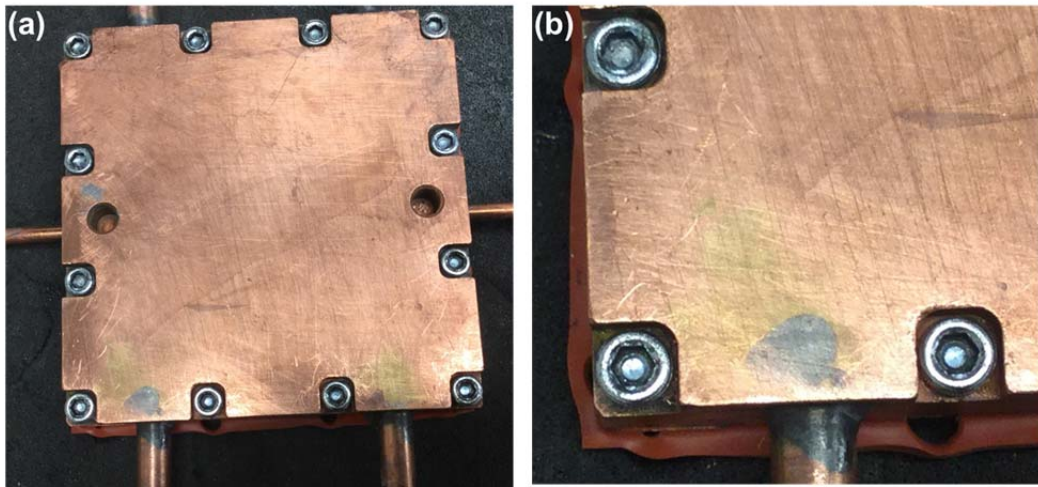
Figure 7. (a) Deformed 60A silicone gasket after chamber assembly; (b) enlarged lower left corner.

4.3.2   Vacuum Performance of Gasket Materials

The capability of the gasket material to sustain vacuum during a freeze-thaw cycle was tested and the results are presented in Figure 8. Note that the initial and final pressure readings were at steady state. The transient pressure readings were not steady-states ones, and these readings were nominal. The sealed but uncharged chamber was first evacuated by a vacuum pump. During the freeze-thaw cycle, the dry chamber was cooled from room temperature to -4°C, and then heated to 49°C, and finally cooled back to room temperature. At the initial and final temperatures, which were within 1°C of each other, the gauge pressure was measured and

the loss of vacuum was quantified as $\Delta P = P_{g,f} - P_{g,i}$. Without any working liquid, this test was a direct indication of the capability of the gasket material to hold vacuum under different temperatures. The vacuum performance degraded significantly when the condenser was heated up after reaching a freezing temperature. The results in Figure 8 suggested that the thermal stress on the rubber gasket introduced a small air leakage.

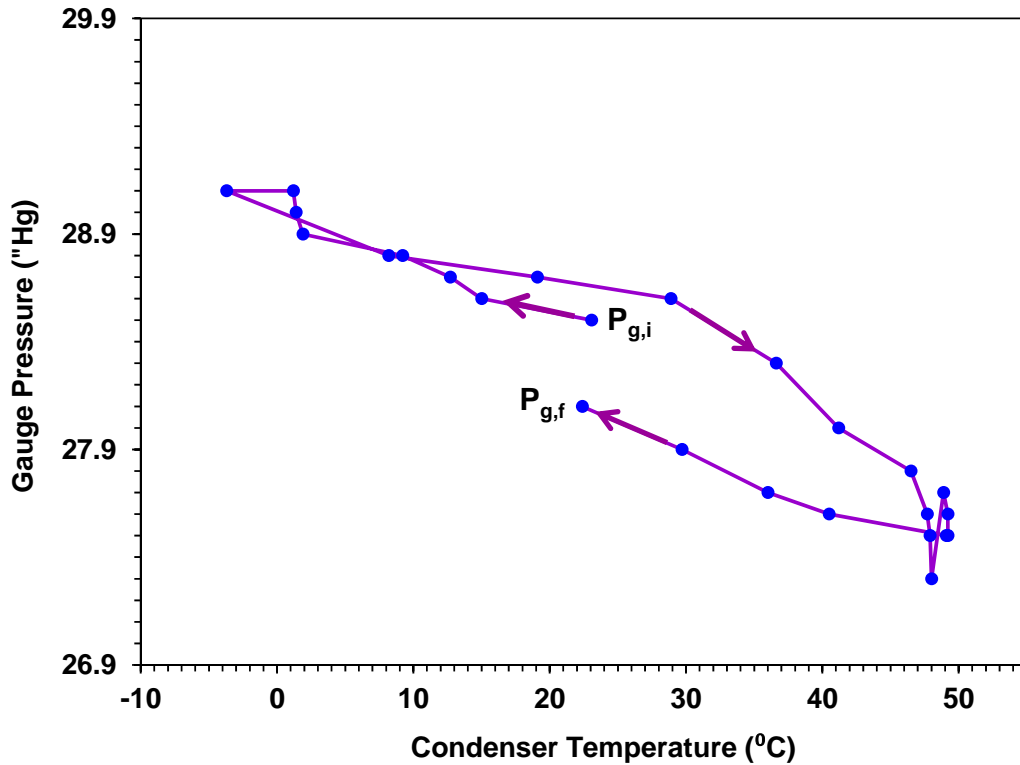**Figure 8.** The vacuum gauge pressure of an *uncharged* chamber as a function of condenser temperature (EPDM 60A gasket).

The gasket materials were compared in Figure 9 in terms of the loss of vacuum defined in Figure 8. Although Silicone 90A exhibited worse vacuum performance than EPDM, Neoprene and Buna both exhibited notably better performances that warrant further investigation with charged vapor chambers.
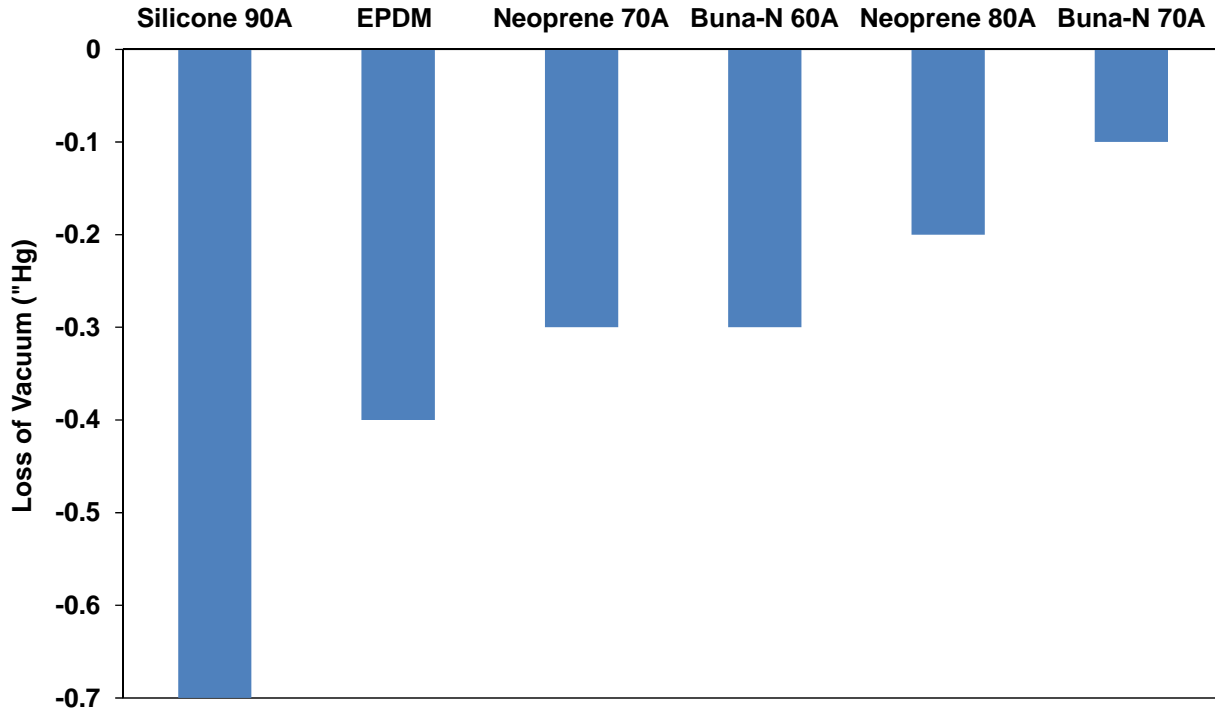
Figure 9. Loss of vacuum (ΔP) for various gasket materials after the freeze-thaw cycle represented by Figure 8.

4.4 Thermal Diode Test after Shipment

After the treatments simulating postal shipment detailed in Section 3.1, the thermal diode was tested for its heat transfer performance in both the forward and reverse modes (Figure 10). In the forward mode, the heater power was up to $Q = 50W$; in the reverse mode, the heater power was only 10W because of the significant temperature rise when the diode behaved as a poor conductor. The diodicity η was calculated using equation (1) with k_f evaluated at 50W and k_r at 10W.

The most important result in Figure 10 was that the packaged diode survived a rigorous shipping test. *After shipment*, the diodicity was tested with the cold plate temperature of $T_0 = 25°C$ or 50°C and an EPDM 60A gasket. The diode survived the shipping test, with the diodicity $\eta = 27$ at $T_0 = 50°C$ and $\eta = 20$ for $T_0 = 25°C$. Note the removal of noncondensable gases has not been optimized, so the diodicity could be further improved [1, 4]. The diodicity was improved at a higher chamber temperature mainly because of the significant increase in the forward conductivity. Note this diodicity was not as high as our prior results of $\eta \geq 100$, because we did *not* completely evacuate the noncondensable gases, e.g. by using the maximum allowable number of secondary vacuums [4]. Although such an optimization is relatively easy to accomplish, it was not the focus of this study centered on the freeze-thaw behavior.
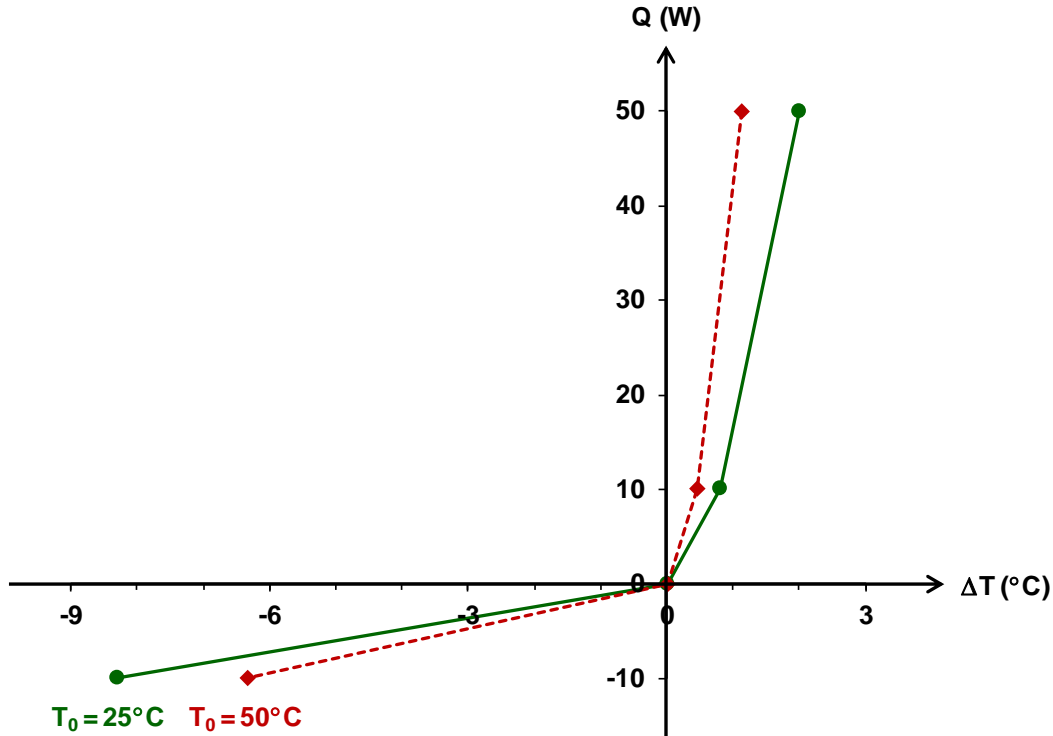
Figure 10. Thermal diode test after shipment (EPDM 60A gasket).

4.5 Thermal Diode Testing after Freeze-Thaw

4.5.1 Freeze-Thaw Test with Buna-N Gasket

Despite encouraging results after shipment (Figure 10), the performance of the thermal diode significantly degraded after a freeze-thaw cycle. Based on the vacuum performance of flat gaskets in Figure 9, Buna-N 70A was the most promising gasket material. The Buna-N 70A gasket was adopted in the freezing test in Figure 11.

In Figure 11, significant degradation was still observed with the Buna-N 70A gasket after freezing. The freezing was accomplished by imposing $T_0 = -10°C$, leading to an average chamber temperature as low as -5°C. The diodicity was $\eta = 8.6$ before freezing, but only $\eta = 2.4$ after freezing, both measurements were taken when the cold plate was steady at $T_0 = 25°C$. We shall note again that the diodicity can be improved by secondary vacuums to more completely remove the noncondensable gases [4], but such an optimization was not the focus of this study. The degradation in diodicity was mostly due to the sharp decrease in the forward effective conductivity. The sharp decrease was consistent with leakage of noncondensable gases, which are known to inhibit condensation heat transfer [4]. The leakage hypothesis was further tested below.
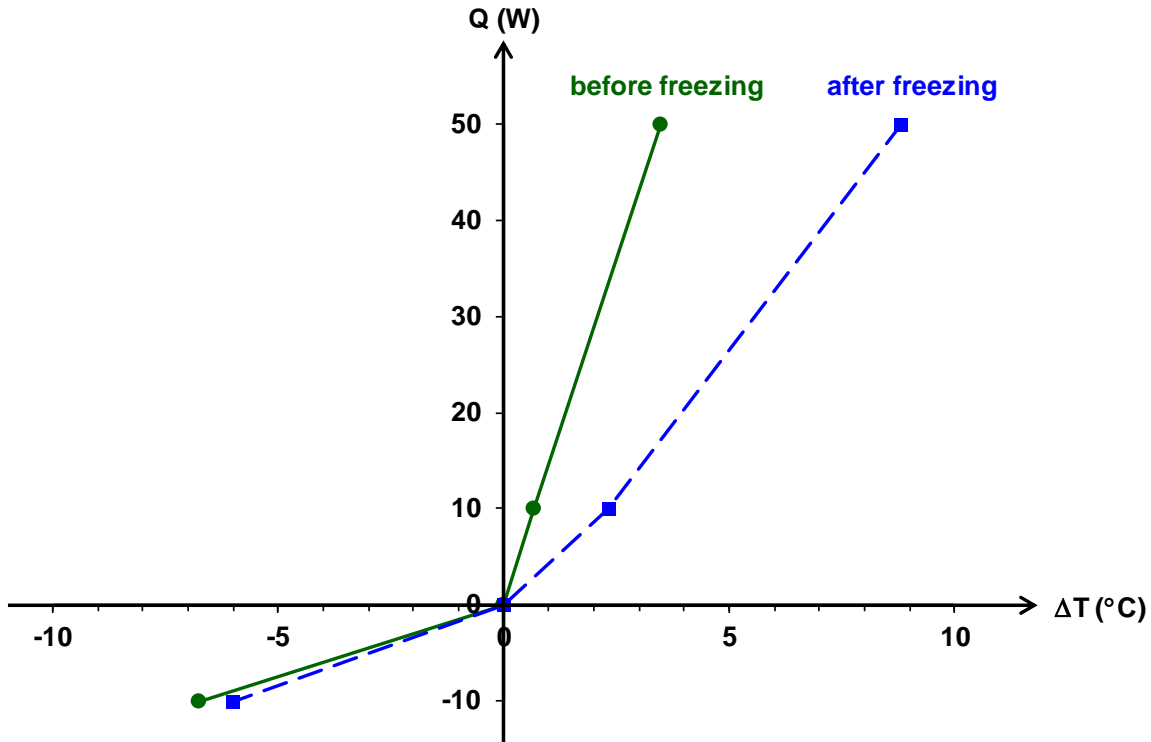
Figure 11. Thermal diode test before and after freezing (Buna-N 70A gasket).

4.5.2   Mechanism of Freeze-Thaw Degradation

To test the hypothesis that the degradation was due to the leakage of noncondensable gases, secondary vacuums were pulled to remove the noncondensables (Figure 12). After a freeze-thaw cycle, the chamber performance degraded in Figure 12a. However, upon brief vacuum pulling in Figure 12b, the chamber performance returned back to (and actually above) the pre-freezing value. Note that we only tested the forward-mode performance which was strongly affected by the freeze-thawing. The reverse mode was mainly through vapor conduction and was nearly independent of the freeze-thaw cycle.

The results of freeze-thaw tests are shown in Figure 12. The dashed line shown in Figure 12 is the theoretical limit [4] of the chamber performance corresponding to a wick thickness of 1.0 mm used here. The freeze-thaw tests in Figure 12 have two important implications: (i) *The freeze-thaw cycle appears to introduce leakage of noncondensable gases*. This hypothesis is consistent with both the initial degradation in performance (Figure 12a) and subsequent rejuvenation via successive evacuations (Figure 12b). This hypothesis is further corroborated by the uncharged chamber test in Figure 8, where the loss of vacuum indicated air leakage. (ii) *Both the superhydrophilic and superhydrophobic surfaces can survive exposure to freezing temperatures*. If this was not the case, vacuum-pulling after the freeze-thaw cycle would not return the chamber performance to the pre-freezing level in Figure 12.
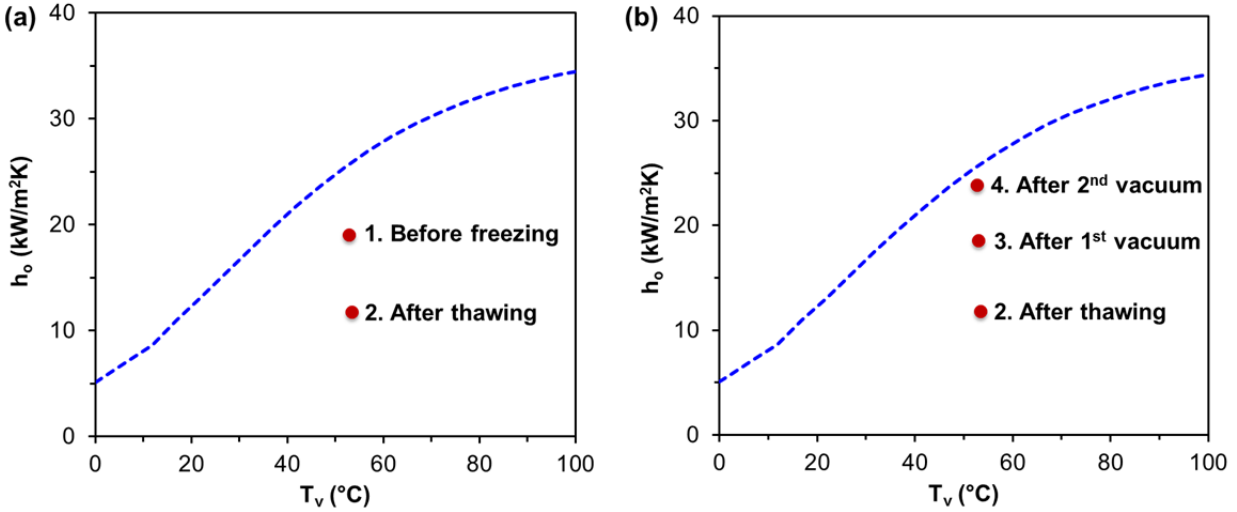
Figure 12. Overall heat transfer coefficient (h_o) of the jumping-drop diode in the forward mode (EPDM 60A gasket): (a) After a freeze-thaw cycle (1→2) and (b) After two successive evacuations (2→3→4)

5 CONCLUSIONS

- *The galvanic superhydrophobic and sintered superhydrophilic surfaces survived a freeze-thaw cycle.* Although a major concern at the beginning of this study, the durability of the superhydrophobic surface was confirmed by our tests. In the future, repeated freeze-thaw cycles should be introduced to study long-term durability for space applications.

- *The flat gasket for vacuum seal introduced leakage of noncondensable gases after a freeze-thaw cycle.* Although the flat gasket design worked fine at room temperature and above, it was not suitable under freezing conditions. The inadequacy of the flat gasket was verified on many alternative materials such as EPDM, Buna-N and Neopreene. In the future, O-rings should be evaluated instead of flat gaskets, perhaps with a material exhibiting good vacuum performance as identified in this study.

- *The present thermal diode design after a crimp-seal survived the shipping test*, including repeated dropping to the ground in a postal package.

REFERENCES

1.   Boreyko, J., Zhao, Y., and Chen, C., "Planar Jumping-drop Thermal Diodes," *Appl. Phys. Lett.*, Vol. 99, Article No. 234105, 2011.

2.   Boreyko, J. and Chen, C., "Self-propelled Dropwise Condensate on Superhydrophobic Surfaces," *Phys. Rev. Lett.,* Vol. 103, Article No. 184501, 2009.

3.   Larmour, I., Bell, S., and Saunders, G., "Remarkably Simple Fabrication of Superhydrophobic Surfaces Using Electroless Galvanic Deposition," *Angew. Chem., Int. Ed.*, Vol. 119, pp. 1740-1742, 2007.

4.   Boreyko, J. and Chen, C., "Vapor chambers with jumping-drop liquid return from superhydrophobic condensers," *Int. J. Heat Mass Transfer*, Vol. 61, pp. 409-418, 2013.

5.   Hao, T., Ma, X., Lan, Z., Li, N., and Zhao, Y., "Effects of superhydrophobic and superhydrophilic surfaces on heat transfer and oscillating motion of an oscillating heat pipe," *J. Heat Transfer*, Vol. 136, Article No. 082001, 2014.

6.   Labconco freeze dry system (FreeZone 77500) product manual. Available at http://www.labconco.com/literature/manuals/freeze-dry-systems (accessed prior to 2/12/2016).

7.   "NASA Practice No. PD-ED-1223: Vacuum seals design criteria," Available at http://oce.jpl.nasa.gov/preferred_practices.html (accessed prior to 2/12/2016).

LIST OF SYMBOLS, ABBREVIATIONS, AND ACRONYMS

Buna-N	o ring material
ΔP	delta pressure (losss of vauum)
ΔT	delta temperature
EPDM	ethylene-propylene-diene monomer
η	diodicity
A_w	wick area
h_o	overall heat transfer coefficient
H	total thickness of wick structure and vapor spacing
H_w	thickness of copper wick
k_w	thermal conductivity of copper wick
NASA	National Aeronautics and Space Administration
$P_{g,f}$	final gauge pressure
$P_{g,i}$	initial gauge pressure
Q	heater power
T_o	circulating fluid temperature

DISTRIBUTION LIST

DTIC/OCP
8725 John J. Kingman Rd, Suite 0944
Ft Belvoir, VA 22060-6218   1 cy

AFRL/RVIL
Kirtland AFB, NM 87117-5776   2 cys

Official Record Copy
AFRL/RVSV/Andrew Williams   1 cy

(This page intentionally left blank)